03 May 2013, 2:50 pm - 3:05 pm

Dem Modelling of Granular Materials During Cyclic Loading

J. S. Vinod
University of Wollongong, Australia

Buddhima Indraratna
University of Wollongong, Australia

T. G. Sitharam
Indian Institute of Science, India

Commemorate the Legacy of Ralph B. Peck
April 29 - May 4, 2013 CHICAGO
Seventh International Conference on
Case Histories in Geotechnical Engineering
and Symposium in Honor of Clyde Baker

DEM MODELLING OF GRANULAR MATERIALS DURING CYCLIC LOADING

J S Vinod
University of Wollongong
NSW 2522 Australia

Buddhima Indraratna
University of Wollongong
NSW 2522 Australia

T G Sitharam
Indian Institute of Science
Bangalore, India

ABSTRACT

This paper summarises the potential of the Discrete Element Method (DEM) to simulate the behaviour of granular materials under cyclic loading conditions. DEM simulations were carried out on two different assemblies of granular particles (e.g. sand and ballast). It is shown that DEM is capable of simulating the cyclic behavior of granular materials (e.g. liquefaction, post liquefaction and cyclic densification of ballast) similar to the laboratory experiments. Moreover, an instrumented track at Bulli, NSW, Australia, was modeled using DEM to examine the lateral movement of granular materials, including the particle breakage during cyclic loading. The results of these simulations captured the lateral response of ballast in accordance with the field observations and the evolution of micro-mechanical parameters such as a distribution of the contact force and bond force developed during cyclic loading is presented to explain the mechanism of particle breakage.

INTRODUCTION

Granular materials such as sand and ballast exhibit complex behaviour (e.g. liquefaction, stiffening and densification) during cyclic loading that are primarily due to changes in the effective stress, caused by different drainage boundaries, which affect the serviceability of the structure. One of the major concerns during cyclic loading (e.g. earthquake) is to safe guard the structure from liquefaction, particularly if the structures are resting on loose saturated sand. Often, costly ground improvement techniques (e.g. the densification of sand) are needed to mitigate the liquefaction hazards including earthquake induced displacements. Despite the extensive research in this area (e.g. Lee and Seed, 1967; Seed and Peacock, 1971; Ladd, 1974; Tatsuoka et al., 1982; Ishihara, 1985; Yoshimi et al 1989; Talaganov, 1996; Chein, 2002 and Sitharam and Vinod, 2008) liquefaction still remains a major problem even in recent earthquakes. The important information required to evaluate earthquake induced displacement is the undrained stress-strain response of post liquefied sands. This will allow the designer to predict the potential resistance of liquefied sand to withstand the monotonically increasing static loads. Recent laboratory investigations (e.g. Toyoto et al 1995; Vaid and Thomas, 1995; Kukusho et al 2005 and Sitharam et al 2009) have led to a qualitative understanding of the post liquefaction undrained behaviour of sandy soils. However, no attempt has been done so far to understand the mechanism and factors influencing the post liquefaction behaviour at the grain scale level.

Similarly, ballast undergoes high permanent deformation and densification during drained cyclic loading. For instance, cyclic loads from heavy haul trains degrade and foul the ballast, directly contributing to track settlement. An understanding of how ballast reacts during cyclic loading plays a key role in reducing the maintenance costs of railway tracks while optimising passenger comfort.

Numerous research studies have recently been carried out to understand the behaviour of ballast during cyclic loading (e.g. Shenton 1975; Raymond and Williams 1978; Alva-Hurtado and Selig 1981; Jeffs and Marich 1987; Indraratna et al. 1998; Salim and Indraratna 2004; Indraratna et al. 2005; Indraratna and Salim 2005; Lackenby et al. 2007; Anderson and Fair 2008 and Indraratna et al, 2010). However, laboratory investigations and field assessments alone cannot provide a full insight into complex ballast breakage mechanisms and associated deformation when the discrete and heterogeneous nature of granular materials is considered. Recently, DEM software PFC^{2D} has been used to study the behaviour of ballast under cyclic loading while incorporating particle breakage (e.g. Lobo-Guerrero and Vallejo 2006; Hossain et al. 2007). Since the complex micro-mechanics of ballast materials have not been studied before, the mechanics of particle breakage and its influence on the cyclic densification needs a thorough

examination.
For this reason it is important to comprehensively understand the macroscopic behavior and the micromechanical response of granular material during cyclic loading. This can be easily be achieved by particulate modelling approaches. In this direction, early attempts to observe the distribution of force and particle behaviour at microscopic levels were made by Dantu (1957) and Wakabayashi (1957) using optically sensitive materials. Later on De Josselin de Jong and Verruijt (1969) analyzed force distribution in such assemblies, studying individual particles. The results of these experiments provided a qualitative understanding of the mechanisms of load transfer and the deformation characteristics of granular materials. New experimental techniques (Desrues et al 1996) using computer tomography have also provided important information about the evolution of the fabric. However, these analytical models were applicable only for regular arrays of spheres and discs of uniform size under simple loading. Not only that, these tests are expensive and time consuming, and the data extracted is insufficient for micromechanical analysis. One solution to this difficulty is computer simulated numerical experiments which offer complete information of all the microscopic features for detailed analysis. One such numerical technique is the Discrete Element Method (DEM) pioneered by Cundall and Strack (1979). DEM models the soil as discrete particles interacting through contact forces without any assumptions of continuum, while the isotropy and macro behaviour is obtained from the micro response at the contacts. An accurate measurement of the contact forces and displacement is possible and sufficient micro-parameters data can be extracted for micro-mechanical analysis. In this study therefore, DEM modelling has been used to simulate liquefaction, post liquefaction, permanent deformation, and the degradation of granular materials during cyclic loading. The macroscopic results for all the numerical simulations are presented along with micromechanical explanations in terms of the average coordination number and distribution of the contact force. The aim is to gain an insight into the microscopic behaviour and bridge the gap in understanding the macro behaviour from the micro response

DISCRETE ELEMENT METHOD (DEM)

The DEM is an explicit finite difference program. The interaction of the particles is treated as a dynamic process where a state of equilibrium develops whenever the internal forces balance. The equilibrium contact forces and displacement of a stressed assembly are found through a series of calculations that trace the movements of the individual particles. These movements are the result of a propagation of disturbances through the particle system caused by specified wall and particle motion or body forces. This is a dynamic process where the speed of propagation depends on the physical properties of the discrete system. It will also allow finite displacement and rotation of discrete bodies, including complete detachment, and will automatically recognise new contacts as the calculation progresses.
The calculations performed in DEM alternate between the application of Newton's second law to the particles, and a force displacement (i.e. constitutive) law at the contacts (Fig.1). Newton's second law is used to determine the motion of each particle arising from the contact and body forces acting upon it, while the force displacement law is used to update the contact forces arising from the relative motion at each contact.
This dynamic behaviour in DEM is represented by a time stepping algorithm where the velocities and accelerations are assumed to be constant within each time step. DEM is based on the idea that the time step chosen may be so small that during a single time step, the disturbance cannot propagate further from any particle than its immediate neighbours. Then, at all times, the forces acting on any particle are determined exclusively by its interaction with the particles with which it is in contact. The DEM software (e.g. TRUBAL & PFC^{2D}) models the movement and interaction of the stressed assemblies of spherical particles. The distinct particles are displaced independently from one another and only interact at contacts or interfaces between the particles. The particles are assumed to be rigid and have negligible contact areas (contact occurs at a point), but they are, allowed to overlap at the contact points using the soft contact algorithm. PFC^{2D} enables the investigation of features that are not easily measured in laboratory tests such as co-ordination numbers, inter-particle contact forces, and the distribution of normal contact vectors to be investigated, and it is also possible to compose bonded particles into agglomerates and simulate fracture when the bonds break.

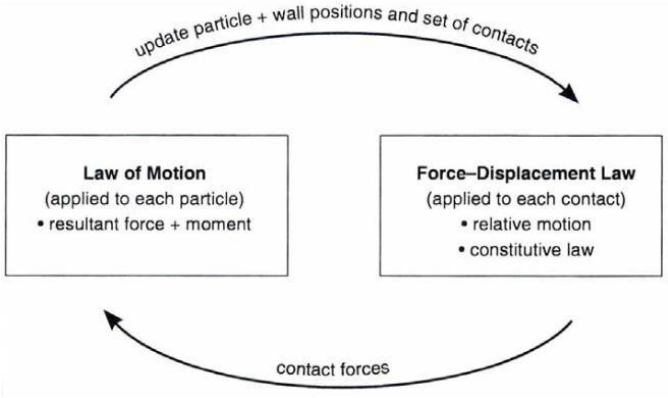

Fig.1: Calculation cycle used in PFC2D (Itasca, 2004)

NUMERICAL PROCEDURES

Numerical Simulations of the liquefaction and post liquefaction behaviour of granular materials has been carried out using TRUBAL (3 D version). An assembly of 1000 spheres with particles varying in size from 0.2 to 2 mm was considered (Fig.2) and a linear force displacement contact model was used for the numerical simulation program. The stiffness of the spherical particles in the linear contact model was evaluated by assuming the same strain (δ/d) for the Hertzian and linear contact model (Vinod, 2006 and Sitharam et al 2009). The particles were assigned a Young's modulus

of 70 GPa; Poisson's ratio of 0.3; density of 2650 kg/m^3 and a contact friction value of 0.5. The inset of Fig. 2 shows the assembly that was initially generated without any overlap in a cubic space having a periodic space boundary. After generation the assembly was isotropically compacted to a desired initial confining pressure, and then a series of undrained strain controlled cyclic triaxial numerical simulations were carried out on these samples at a frequency of 1.42 Hz. Undrained tests were carried out by keeping the volume constant throughout the shearing process. After initial liquefaction, which is defined as the state at which the excess pore water pressure becomes equal to the initially applied confining pressure, undrained monotonic tests were carried out on samples without dissipating the excess pore water pressure developed during initial liquefaction.

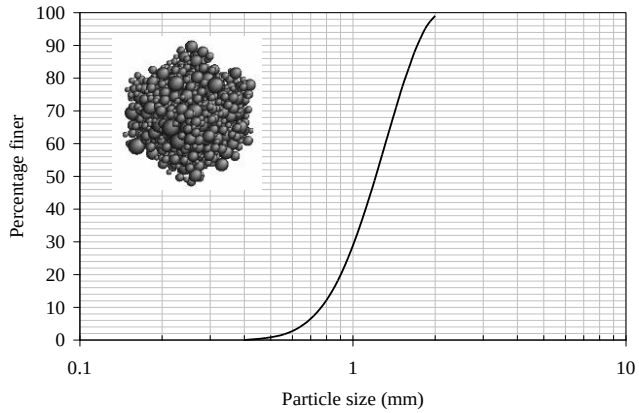

Fig.2: Particle size distribution of sand; Inset (a) Initially generated assembly of spheres

PFC ^{2D} Modelling of ballast particles

A new approach was used to model an identical two dimensional (2D) projection of the ballast particles. Fifteen representative ballast particles (3 from each sieve size range) of different shapes (almost rectangular, circular and triangular) were selected. The sieve sizes considered were: (i) passing 53 mm and retaining 45 mm, (ii) passing 45 mm and retaining 37.5 mm, (iii) passing 37.5 mm and retaining 31.5 mm, (iv) passing 31.5 mm and retaining 26.5 mm, and (v) passing 26.5 mm and retaining 19 mm. The photographs of each of the selected ballast particles were taken and the images were imported into AutoCAD in a single layer. The images were then filled with tangential circles in another layer and every circle was given an identification number (ID). The identification number (ID), radius and central coordinates of each circular particle were extracted from AutoCAD in order to generate 'Balls' in PFC^{2D}. Table 1 shows the picture of typical ballast particles created for the numerical simulation. These irregular particles were assigned name such as R1, R2, and R3 etc.

Table.1: Representative ballast particles (Indraratna et al 2010a)

Ballast Particles	PFC Particles
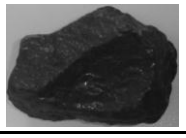	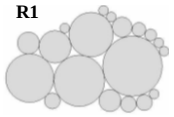 R1
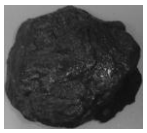	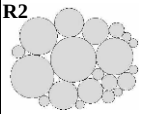 R2
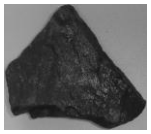	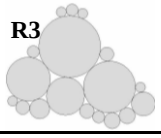 R3

Subroutines were developed in PFC^{2D} after gathering the ID, the radius, and coordinates of the centre of each circular particle representing angular ballast particles. These subroutines were used in the main program to generate irregular ballast particles. A 300mm wide × 600mm high biaxial cell, similar in size to the laboratory equipment, was generated for the numerical simulation. A typical sample considered for the cyclic biaxial tests and track modelling is shown in Figure 3. Table 2 lists the micromechanical parameters adopted for the DEM simulations. A linear contact model was used for the numerical simulation program. The biaxial sample generated was given a confining pressure of 60 kPa.

Specimen preparation

The particle size distribution (PSD) adopted in this simulation is shown in Fig.3. Sub-routines were developed (using the FISH Language) in PFC^{2D} to generate irregular ballast particles and filler particles. In order to achieve the specified porosity, the biaxial cell was filled with some more circular particles (filler particles).The inset of Fig.3 shows the initially generated bi-axial sample having a size similar to the laboratory specimen.

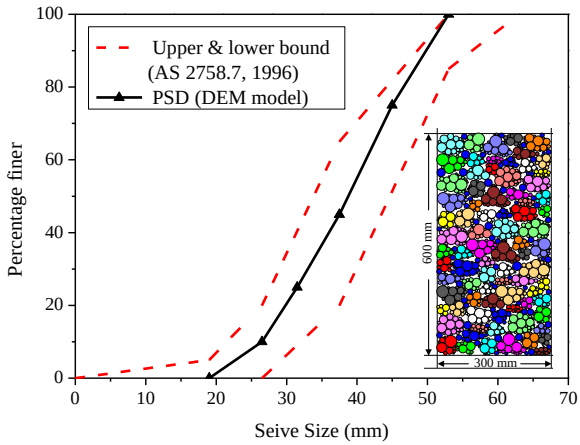

Fig.3: Particle size distribution of ballast; Inset (a) Initially generated irregular ballast samples

A subroutine was developed to apply a stress-controlled cyclic biaxial test at the desired frequency (f) and amplitude of cyclic loading. The minimum cyclic stress (q_{min}) was kept at 45 kPa which represents the unloaded state of the track (such as the weight of sleepers and rails) (Lackenby et al. 2007). The cyclic deviatoric stress (q_{cyc}) applied to the ballast that correspond to various frequencies were estimated in accordance with Esveld (2001). Cyclic biaxial tests at a frequency of 10 Hz, 20 Hz, 30Hz and 40 Hz were simulated. Data such as axial strain (ε_a), bond breakage (B_r) were recorded at every number of cycles (N). The parameters used for the biaxial simulation are shown in Table.2.

Table 2: Parameters used for the DEM simulations (Indraratna et al. 2010a)

Micromechanics parameters	Values
Particle density (kg/m^3)	2500
Radius of particles (m)	$16\times10^{-3} - 1.8\times10^{-3}$
Interparticle & wall friction	0.5
Particle normal & shear stiffness (N/m)	3×10^8
Side wall Stiffness (N/m)	3×10^7
Top & bottom wall stiffness (N/m)	3×10^8
Parallel bond normal & shear stiffness (N/m)	6×10^{10}
Parallel bond normal & shear strength (N/m^2)	5×10^6

RESULTS AND DISCUSSION

Liquefaction and Pore Pressure Response

Fig. 3 presents the variation of deviator stress with mean p for an isotropically compressed assembly at an axial strain of 0.6 %. As Fig. 3 shows with the application of a constant cyclic strain amplitude (say 0.6 %), the deviator stress slowly decreases with mean p due to the development of excess pore water pressure (Fig. 4). Finally, the deviator stress reaches zero as the pore water pressure ratio ($U = u/\sigma_3$) reaches one (the condition for initial liquefaction). In a qualitative sense, the results of the numerical simulation captured the realistic behaviour of liquefaction observed in the laboratory experiments.

Figure 4 shows the plot of the average coordination number and excess pore water pressure with the number of cycles. The average coordination number $Z = M/N$, of the assembly is defined as the ratio of the total number of contact points (M) within the assembly volume (V) to the total number of particles (N) in the assembly. The pore water pressure has been computed while considering the difference in the mean pressure between the undrained (effective) and drained (total) stress path during strain controlled cyclic triaxial tests. A steady decrease in the average coordination number with an increase in N can be observed (Fig. 4). This steady decrease in the average coordination number is due to the development of excess pore pressure during constant cyclic strain loading in an undrained condition. The average coordination number decreased dramatically at a value close to 3, which corresponds to the collapse of the soil structure.

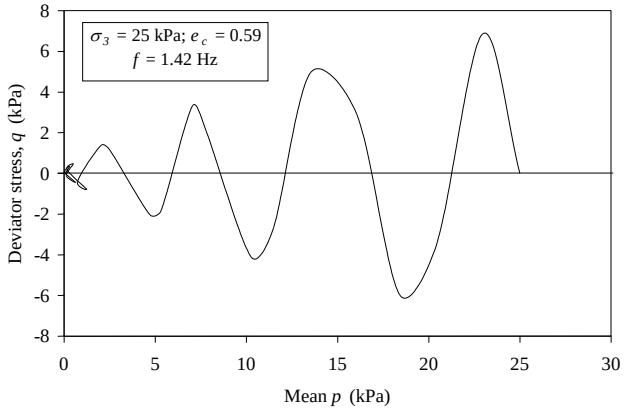

Fig 3. Variation of deviator stress with mean p (Sitharam and Vinod, 2008)

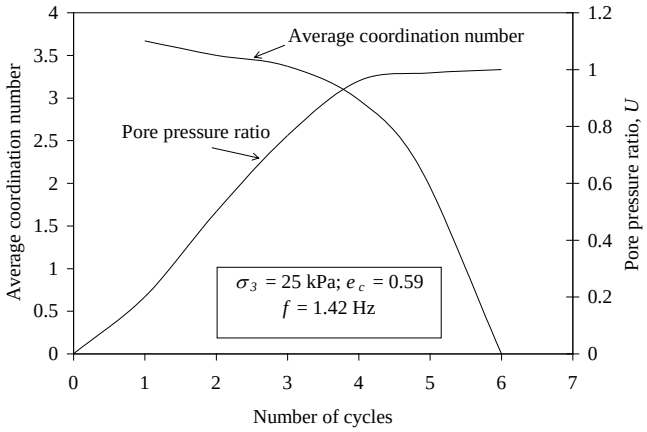

Fig. 4. Variation of average coordination number with number of cycles (Sitharam and Vinod, 2008).

A combined analysis of the shear strain and number of cycles for liquefaction for the range of confining pressure and void ratio is presented in Fig 5. The results of the numerical simulation were also compared with the strain controlled laboratory experimental results carried out by Talaganov (1996) and GovindaRaju (2005). It is evident that a unique relationship exists between shear strain and number of cycles for initial liquefaction for the range of void ratio and confining pressure considered for this study. Moreover it is apparent that the results of the numerical simulation are close to the laboratory experimental investigation conducted in the laboratory.

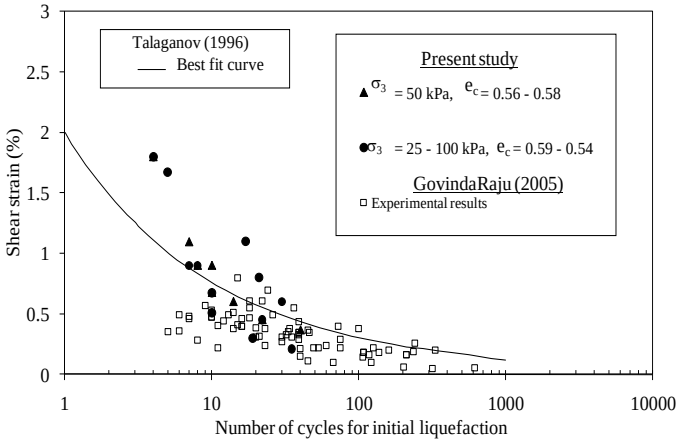

Fig. 5: Variation of shear strain with number of cycles for initial liquefaction (Sitharam and Vinod, 2008).

POST LIQUEFACTION RESULTS

Fig.6 shows the results of post liquefaction undrained monotonic response of sand samples liquefied at different axial strain amplitude (ε = 0.3%, 0.5% & 0.6%) for a confining pressure of 100 kPa prior to initial liquefaction. It is evident from Fig.6 that there is a pronounced influence of cyclic strain amplitude on the post liquefaction monotonic strength of sand. All the samples exhibit an initial deformation with zero deviator stress up to a particular value axial strain, but, with further shearing, a gradual building up of the deviator stress with increase in the axial strain is observed. This may be attributed to the development of negative pore water pressure. Moreover, rate of increase of post liquefaction monotonic strength increases with decrease in the cyclic strain amplitude. This may be due to the effect of cyclic strain on the soil fabric at liquefaction. During the undrained monotonic loading, on the liquefied samples, the deformation required to form a completely new soil fabric arrangement to bear the deviator stress increases with increase in the amplitude of axial strain prior to liquefaction. Similar laboratory results have been reported by Vaid and Thomas (1995) and Kukusho et al. (2004).

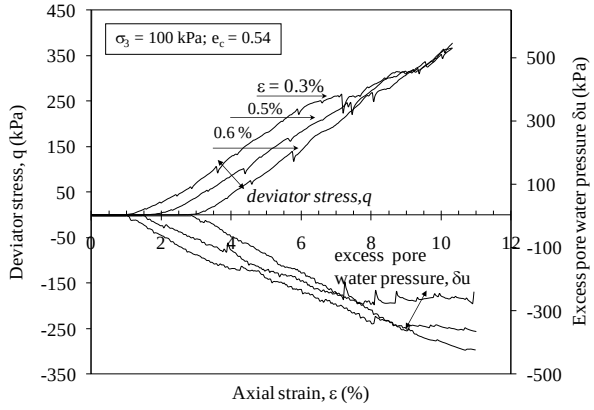

Fig.6: Variation of deviator stress and excess pore water pressure with axial strain for different amplitude of axial strain prior to liquefaction (Sitharam et al., 2009).

Fig. 7 presents the variation of the average coordination number with axial strain at a confining pressure of 100 kPa for different amplitude of axial strain prior to initial liquefaction. Note that the rate at which the average coordination number builds up during monotonic loading depends on the amplitude of axial strain applied prior to liquefaction. It is evident that the rate of building up of average coordination number increases with decrease in the amplitude of axial strain prior to liquefaction. The average coordination number steadily increases from zero (point of liquefaction) to a value of 4 and thereafter remains constant.

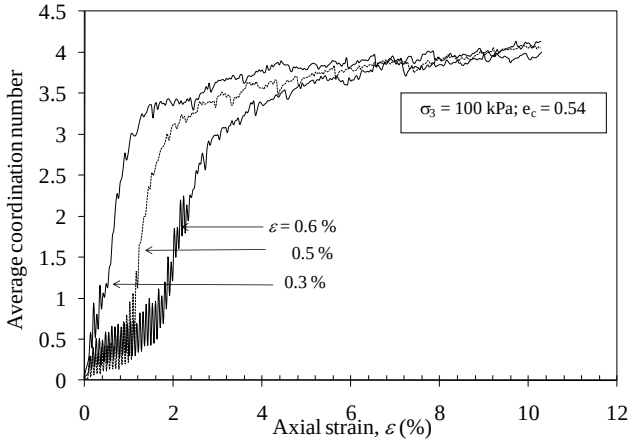

Fig. 7: Plot of average coordination number versus axial strain (Sitharam et al., 2009).

Comparison with Assembly after Dissipating the Excess Pore Water Pressure Developed During Initial Liquefaction

Fig. 8 presents the plot of the stress ratio versus axial strain for samples with and without dissipating the excess pore water pressure generated during cyclic loading. The plot shows a steady increase in the stress ratio from the start of monotonic loading for the assembly after the excess pore water pressure has been dissipated during liquefaction. Whereas the assembly where the excess pore water developed during liquefaction has not been dissipated shows a zero stress ratio up to an axial strain of 3%, after which there is a sudden increase in the deviator stress with axial strain, beyond an axial strain of 3% both assemblies have a unique stress ratio value.

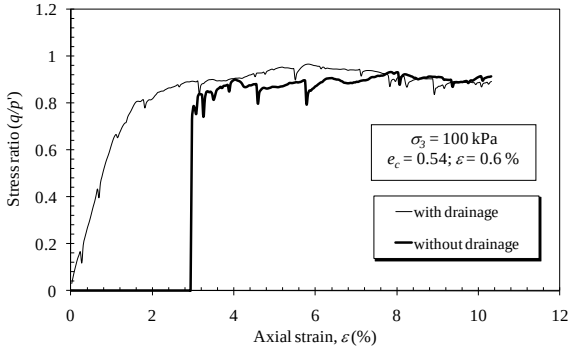

Fig.8: Variation of stress ratio with axial strain for assemblies with and without dissipating the excess pore water pressure developed during cyclic loading.

The variation of the average coordination number with axial strain for samples with and without dissipating the excess pore water pressure during cyclic loading is presented in Fig. 9. Here the average coordination number gradually increases from 3.6 (at zero axial strain) to a constant value of 4 at large strain levels for assembly after dissipating the excess pore water pressure generated during liquefaction. However, the average coordination number increases from zero (point of liquefaction) to 3 at an axial strain of 3 %, and steadily increases to a constant value of 4 at large strain levels. It is interesting to note that both assemblies reach a constant value of the average coordination number at large axial strains (say ε_a > 9 %).

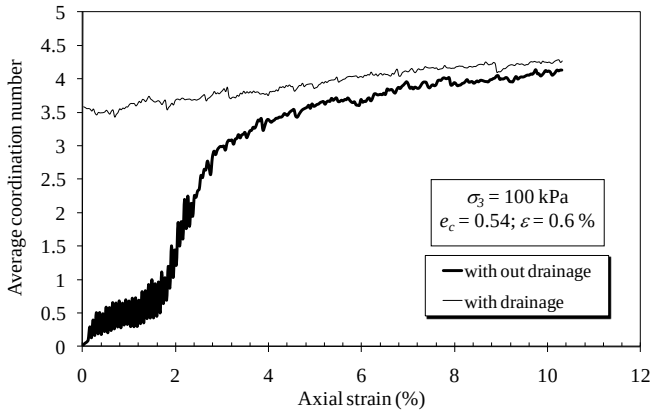

Fig.9: Variation of average coordination with axial strain for assemblies with and without dissipating the excess pore water pressure developed during cyclic loading.

CYCLIC DENSIFICATION BEHAVIOR OF BALLAST

Fig. 10 shows the comparison of axial strain (ε_a) with the number of cycles (N) obtained from the PFC^{2D} and experimental results (Indraratna et al 2010a). It is evident from figure that frequency (f) had a significant influence on ε_a (ε_a increases with f). For a particular value of f, ε_a rapidly increased to maximum value in the initial cycles (e.g., 8% at N=200 for f=30Hz), after which it attained a constant value at a large N. This sudden increase in ε_a at low values of N can be attributed to particle rearrangement and corner breakage. In addition, with an increase in f, higher values of N were required to reach the shake down condition. It is evident from the figure that DEM simulations have captured the similar behaviour similar to that observed in the laboratory experiments.

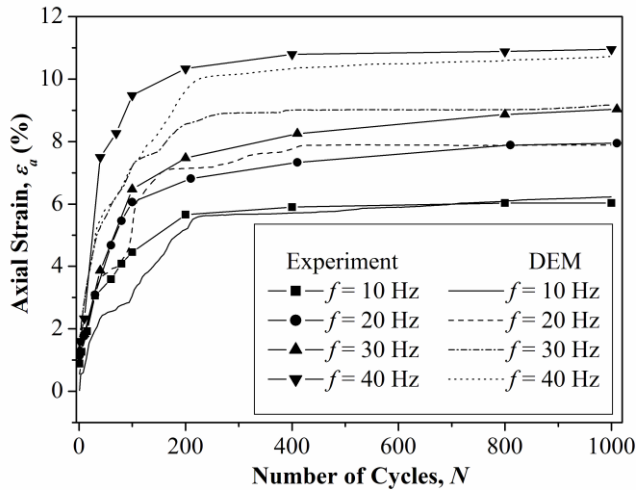

Fig.10 Variation of axial strain (ε_a) with number of cycles for different values of frequency (Indraratna et al 2010a)

Fig. 11 illustrates the variation of broken bonds with the number of cycles for different values of frequency. It is evident that the Br increased with the frequency of cyclic loading (f) and number of cycles (N). It should be noted that all the bonds were broken at initial cycles (around 200 cycles), which highlight the fact that breakage is one of the major factors influencing the development of permanent axial strain (ε_a) at a low N (Fig.10).

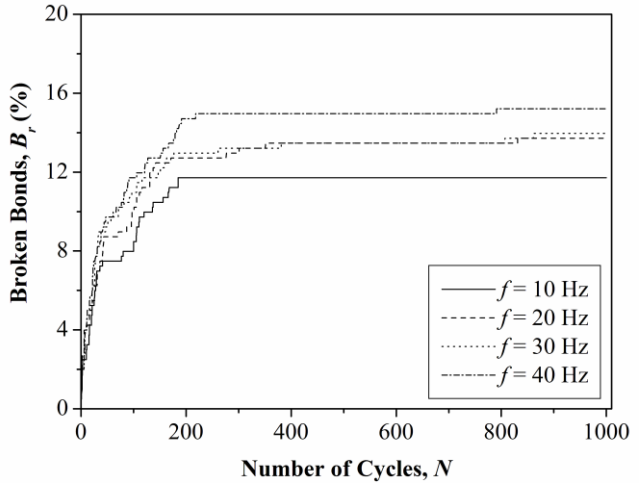

Fig.11: Effects of frequency (f) on bond breakage (Br) with number of cycles (N) (Indraratna et al 2010a)

Fig. 12 presents an enlarged view of particles (Y2) before and after bond breakage (Indraratna et al. 2010). The contact force (CF) of particle Y2 [Fig.12(a)] developed as compressive before breakage. In Fig. 12(b), the CF acting on particles Y2 induced tensile and compressive bond forces in the bond joining particles i and ii. As the cyclic load continued the induced tensile stress exceeded the tensile strength of the particle, causing it to break in tension [Fig. 12(c)]. As can be seen from Fig. 12 (c) and (d), particles i and ii then separated after breakage. CF distribution after breakage is shown in Fig. 12 (d).

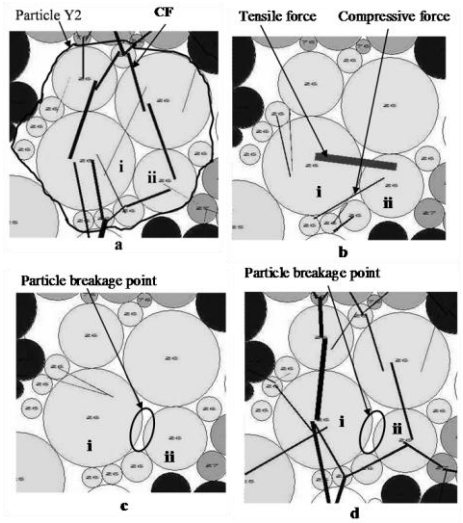

Fig. 12 Details of particle condition: (a) Contact force chains and (b) bond forces before bond breakage; (c) bond forces and (d) contact force chains after bond breakage at 40Hz frequency during cyclic loading (Indraratna et al. 2010a)

Fig. 13 a & b present the variation of displacement vectors during the first and 500th cycles of loading respectively. As expected, the particles rearrange themselves and moves towards the centre under cyclic loading. This results in the development of tensile bond forces between the particles in a cluster. As the cyclic load continues, the induced tensile stress exceeds the tensile strength of the particle causing it to break. This breakage and rearrangement of broken particles contributes towards cyclic densification of the assembly (Fig.13b).

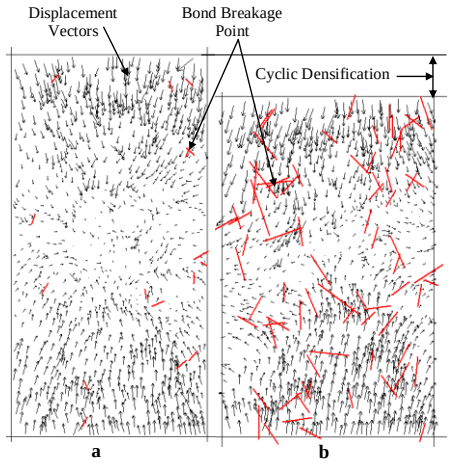

Fig.13: Displacement vectors and bond breakage (a) at 1st cycle of loading (b) at 500 cycle of loading (Pramod et al 2009)

RAIL TRACK SIMULATION USING DEM: A CASE STUDY

The Bulli track was constructed between two turnouts along the South Coast of New South Wales. A field trial was conducted on an instrumented track at Bulli, with the specific aims of studying the benefits of a geocomposite installed at the ballast-capping interface, and to evaluate the performance of moderately graded recycled ballast compared to the traditional uniform fresh ballast (Indraratna et al 2010b). The instrumented track was divided into four 15m long sections. Fresh ballast, fresh ballast with geocomposite, recycled ballast with geocomposite and recycled ballast were used at sections 1 to 4, respectively. To measure the vertical and horizontal deformations of the ballast, settlement pegs and displacement transducers were installed in different track sections. The field measurements were conducted up to 7x10^5 cycles. Detailed explanations of the field testing equipment and experimental procedures are found elsewhere (Indraratna et al., 2010b).

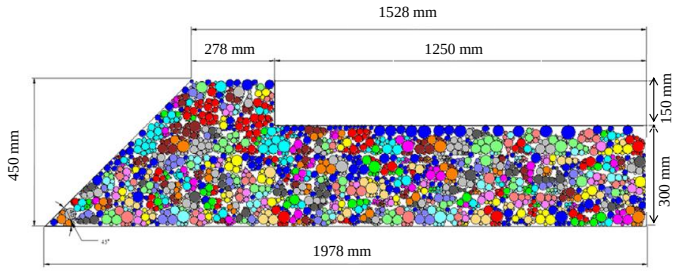

Fig. 14: Initial assembly of the half track model on the Bulli track (Han, 2012)

To understand the micromechanical behaviour of ballast under cyclic loading in a railway track environment, a half track model was developed using DEM. Due to high computational demand associated with the number of particles, only half of the Bulli track was modeled in PFC^{2D}. The initial assembly of the particles and geometry of the track are shown in Fig.14. Table 2 presents the micromechanical properties applied to the DEM model.

Fig. 15 shows the location of the sensors used to measure deformation in the modelled track and they are similar to the instrumented Bulli track. An average measurement was adopted to record the response of the ballast at these locations during cyclic loading. There is a trapezoidal cell with a closed top wall, and three other walls packed with the initial assembly. The sloping side wall (wall 1) was treated as a free boundary while the other walls acted as boundary constraints. To conduct cyclic loading, the velocity of the closed top wall was controlled by a numerical servo-mechanism to maintain the specified force on the loading platen. The bottom wall (wall 2) and right hand side wall (wall 3) were fixed. The stresses and strains were determined by summing the forces acting upon, and the relative distance between the appropriate walls.

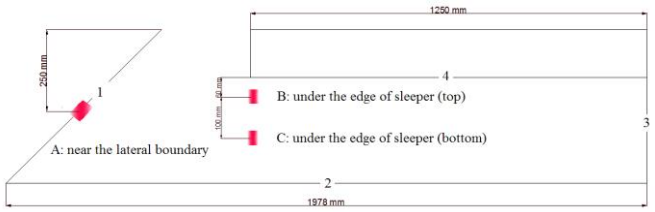

Fig.15: Location of measured points in DEM simulation (*Han, 2012)*

The stresses were computed by taking an average of the values acting on each set of opposite walls, where the stresses on each wall were computed by dividing the total force by the appropriate length of the sample. The strains in both the X and Y directions were calculated using the relationship:

$$\varepsilon = \frac{L - L_0}{L_0}$$

where L is the length and L_0 is the original length in that direction.

A cyclic test at a frequency of 20 Hz was simulated. The lateral strain (ε_x), number of cycles (N) and the bond breakage (B_r) were recorded at every step.

Permanent Deformation

Fig.16 shows the comparison of lateral strain (ε_x) with the cycle ratio (N/N_{max}) from the DEM predictions and field measurements. The cycle ratio (N/N_{max}) is defined as the ratio of the number of cycles (N) at any time, t, to the number of cycles (N_{max}) at the end of the simulation/test. N/N_{max} was used to compare the DEM results with the field assessment. Due to the large computation time, the DEM simulations were carried out at up to 1000 cycles.

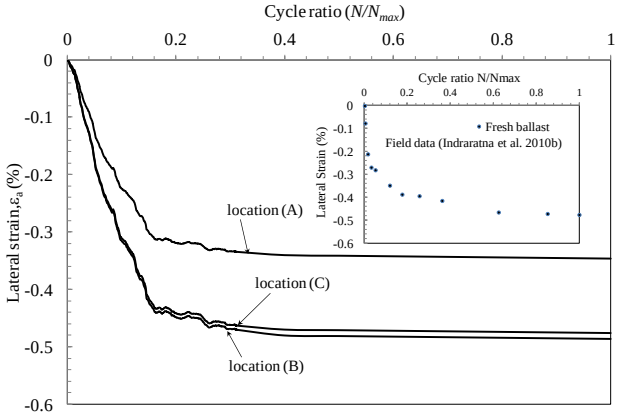

Fig.16: Variation of lateral strain with cycle ratio; Inset (a) plot of lateral strain with cycle ratio (field data)

It is evident from the Fig.16 that DEM simulations have captured the behavior similar to the field data (Indraratna et al 2010b). The lateral strain (ε_x) increases rapidly in the initial cycles and then remains constant at large values of N. The re-arrangement and breakage of ballast particles may be the main factors for the sudden increase in ε_x at low values of N (Fig.17), while, ε_x varies with its location within the ballast. The ε_x near the boundary at point A, is lower than at the edge of the sleeper (point B), and at the bottom layer (point C). This may be due to the higher particle breakage in close proximity to the edge of the sleeper. This clearly highlight that the breakage of particles may be one of the major factor leading to a rapid increase of lateral strain during the initial cycles of loading (Fig.17).

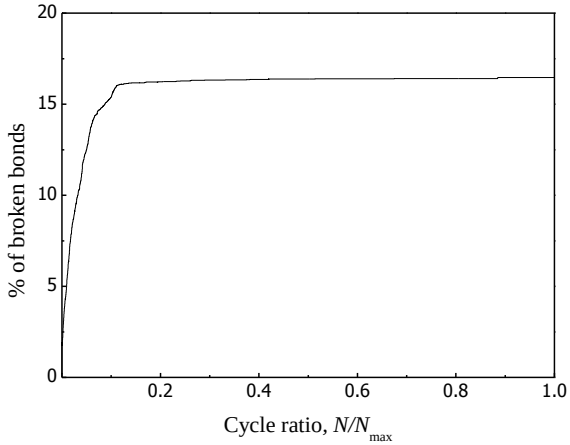

Fig.17: Relationship between bond breakage (B_r) with the cycle ratio (N/N_{max})

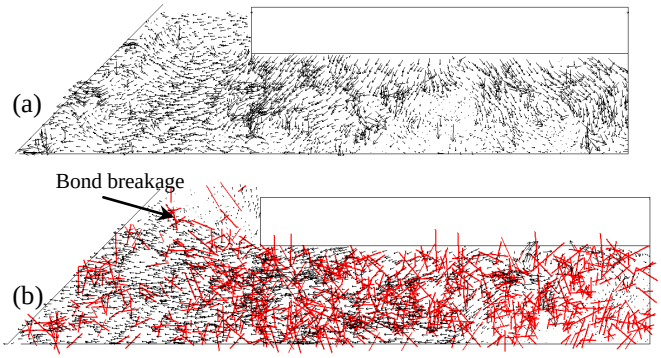

Fig.18: (a) Displacement vectors developed during cyclic loading (N=500) (b) Position of bond breakage at N=500

Fig. 18 a &b illustrates the particle displacement vectors and particle breakage positions during cyclic loading at N= 500. It is evident that the movement of ballast particles under the edge of the sleeper are higher than at other locations (Fig.18 a).

These figures highlight the fact that there is more particle breakage below the sleeper (Fig.18b) than at the lateral boundary. Particle breakage is caused by higher tensile stresses imparted to the ballast during cyclic loading, so when this induced tensile stress exceeds the tensile strength of the particle it break. The re-arragement and breakage of particles are major factors contributing to the permanent deformation of ballast during cyclic loading.

CONCLUSIONS

DEM simulations have captured the realistic behaviour of undrained cyclic response of granular media and have simulated the liquefaction, post liquefaction behavior of granular assembly similar to the laboratory experiments. The DEM results are comparable to the experimental results available in literature and it has captured the effect of different parameters very well. Liquefaction potential of granular material has exhibit a unique relationship irrespective of confining pressure, initial void ratio and amplitude of axial strains. Moreover, the numerical simulations using DEM have qualitatively captured all the features of the post liquefaction undrained behaviour of granular materials that is similar to the experiments. Amplitude of axial strain required for initial liquefaction has a significant influence on the post liquefaction undrained stress strain response.

The DEM simulation also captures the influence of ballast breakage and associated deformation during cyclic loading. A novel approach has been developed to model 2-D shape of real ballast particles using DEM. The DEM based micro-mechanical investigation showed that most particles break during the initial cycles which leads to higher initial axial strains. Particle breakage is mainly due to tensile failure and is concentrated mainly in the direction of the movement of the particles. In addition, it has been found that particle breakage plays a very important role in controlling the development of CF chains in the granular mass during cyclic loading.

The half-track DEM model of the Buli track has captured the lateral response behavior similar to the field studies. Three specific measurement points (i.e., near the lateral boundary, the top layer under the edge of the sleeper, and the bottom layer under the edge of sleeper) similar to the field testing were used in the model. A significant increase in the lateral strains and particle breakage was observed during the initial cycles of loading. The lateral strain and particle breakage near the lateral boundary was much lower compared to the edge of the sleeper.

ACKNOWLEDGEMENT

The authors gratefully acknowledge the contribution of the past research students, Dr Pramod Thakur and Ms. Xu Han to the content of the paper. More elaborate details of the contents discussed in this paper can also be found in previous publications by the first Author and his research students in Geotechnique, International Journal of Geomechanics, International Journal of Geotechnical Engineering since 2007.

REFERENCES

Alva-Hurtado, J. E., and Selig, E. T. [1981]. "Permanent strain behaviour of railway ballast." *Proc., 10th Int. Conf. on Soil Mech. and Found. Eng*., Pergamon Press, New York, 543-546.

Anderson, W. F., and Fair, P. [2008]. "Behaviour of railroad ballast under monotonic and cyclic loading." J. of Geotech. and Geoenv. Eng., Vol.134, No. 3,pp. 316-327.

ASTM. [2002]. "Standard test method for consolidated undrained triaxial compression test for cohesive soils." ASTM D4767-02, ASTM International, West Conshohocken, pp. 923-935.

Chein, K.L, Oh, Y. N, Chang, C. K, [2002], "Effect of fine content on liquefaction strength and dynamic settlement of reclaimed soil", Canadian Geotechnical Journal, Vol. 39, No. 1, pp. 254- 265.

Cundall, P.A. and Strack, O.D.L. [1979], "A Discrete Numerical Model for Granular Assemblies", Géotechnique, 29(1): 47-65.

Dantu, P. [1957], Contibution á l'étude mécanique et géometrique des milieux pulvérulents, *Proc. 4th Int. Conf. Soil Mech. Found. Eng.*, London, Vol.1, pp. 144-148.

De Josselin de Jong, G. and Verrujit, A. [1969], Étude photo-élastique d' un empilement de disques, Cahiers du Groupe Francais de Rhéologie, Vol. 2, No. 1, pp. 73-86.

Desrues, J, Chambon, R, Mokni M., and Mazerolle, F [1996], "Void ratio evolution inside shear bands in triaxial sand specimens studied by computed tomography", Geotechnique, Vol.46, No. 3, pp. 529–546.

Esveld, C. [2001]. "*Modern railway track"*, MRT Press, The Netherlands.

GovindaRaju, L. [2005], "*Liquefaction and dynamic properties of sandy soils"*, Ph.D. thesis, submitted to Indian Institute of Science, Bangalore, India.

Han, X [2012], "*The role of particle breakage on the permanent deformation of ballast*", MS Thesis, University of Wollongong, Australia.

Indraratna, B. [1996]. "Large-scale triaxial facility for testing non-homogeneous materials including rockfill and railway ballast." Aust. Geomech., Vol. 30, pp. 125-126.

Indraratna, B., and Salim, W. [2005]. "*Mechanics of ballasted rail tracks-A Geotechnical Perspective*." Taylor and Francis / Balkema, London, UK.

Indraratna, B., Ionescu, D., and Christie, H. D. [1998]. "Shear behaviour of railway ballast based on large-scale triaxial tests." J. of Geotech. and Geoenv. Eng., Vol. 124, No. 5, pp. 439-449.

Indraratna, B., Lackenby, J., and Christie, D. [2005]. "Effect of confining pressure on the degradation of ballast under cyclic loading." Geotechnique, Vol. 55, No. 4, pp. 325-328.

Indraratna, B., Nimbalkar, S., Cristie, D., Cholachat, R. and Vinod, J. S., [2010b]. "Field Assessment of the Performance of a Ballasted Rail Track with and without Geosynthetics", *Journal of Geotechnical and Geoenvironmental Engineering, ASCE*, Vol. 136, No.7, pp. 907-917.

Indraratna, B., Pramod, K. T. and Vinod, J. S. [2010a]. "Experimental and Numerical Study of Railway Ballast Behaviour under Cyclic Loading", *International Journal of Geomechanics, ASCE*, Vol. 10, No. 4, pp.136 -144.

Ishihara, K. [1985]. "Stability of natural deposits during earthquake", *Proceedings 11th International conference on soil Mechanics and Foundation Engineering*, Vol.1, pp.321-

376.

Itasca [2004]. "*Particle flow code in two and three dimensions*." Itasca Consulting Group, Inc., Minnesota, USA.

Jeffs, T., and Marich, S. "Ballast characteristics in the laboratory." Conf. on Railway Eng., Perth, Australia, pp. 141-147.

Kukusho, T, Hara, T and Hiraoka, R. [2004], "Undrained shear strength of granular soils with different particle gradations", Journal of Geotechnical and Geoenvironmental Engineering, ASCE, 130(6): 621-629.

Lackenby, J., Indraratna, B., McDowell, G., and Christie, D. [2007]. "Effect of confining pressure on ballast degradation and deformation under cyclic triaxial loading." Geotechnique, Vol. 57, No. 6, pp. 527-536.

Ladd, R. S. [1974], "Specimen preparation and liquefaction of sands", Journal of Geotechnical Engineering, ASCE, Vol. 100, No. 10, pp.1180- 1184.

Lee, K.L. and Seed, H.B. [1967], "Cyclic stress conditions causing liquefaction of sand", Journal of Soil Mechanics and Foundations Division, ASCE, Vol.93, No.1, pp. 47-70.

Lobo-Guerrero,S and Vallejo, L.E. [2006], "Discrete element method analysis of railtrack ballast degradation during cyclic loading". Granular Material, Vol. 8, pp.195-204.

Pramod, K. T., Indraratna, B. and Vinod, J. S. [2009], "DEM simulation of effect of confining pressure on ballast breakage", *17th International Conference on Soil Mechanics and Geotechnical Engineering (ISSMGE),* Egypt, 5-9 Oct 2009, Vol.1, pp. 602 – 605.

Raymond, G. P., and Williams, D. R. [1978]. "Repeated load triaxial tests on a dolomite ballast." J. of Geotech. Eng., ASCE, No.7, pp. 1013-1029.

Salim, W., and Indraratna, B. [2004]. "A new elastoplastic constitutive model for coarse granular aggregates incorporating particle breakage." Can. Geotech. J., Vol. 41, No. 4, pp. 657-671.

Seed, H. B and Peacock, W. H. [1971], "Test procedures for measuring soil liquefaction characteristics", Journal of the Soil Mechanics and Foundation Division, ASCE, Vol. 97, No. 8, pp. 1099-1119.

Selig, E. T., and Waters, J. M. [1994]. "*Track geotechnology and substructure management"*, Thomas Telford Services Ltd., London, U.K.

Sitharam, T. G. and Vinod, J. S [2008], "Numerical simulation of liquefaction and pore pressure generation in granular materials using DEM", International Journal of Geotechnical Engineering, 2 (2): 103-113.

Sitharam, T. G., Vinod, J. S. and Ravishankar, B. V. [2009], "Post liquefaction undrained monotonic behaviour of sands: Experiments and DEM simulations", Geotechnique, 29 (9): 739-749.

Standards Australia. [1996]. "Aggregates and rock for engineering purposes." AS 2758.7-96, Standards Australia, Sydney, NSW, Australia, 1-15.

Talaganov, K.V. [1996], "Stress-strain transformations and liquefaction of sands", Soil Dynamics and Earthquake Engineering, Vol.15, pp. 411-418.

Tatsuoka, F., Muramatsu, M and Sasaki, T, [1982], Cyclic undrained stress stain behaviour of dense sands by torsional simple shear tests, Soils and Foundations, Vol. 22, No. 2, pp. 55 -70.

Toyoto, N, Yasuhara, K and Murakami, S and Hyde, A. F. L, [1995], "Post cyclic triaxial behaviour of Toyoura sand", *Proceedings of the First International Conference on Earthquake Geotechnical Engineering*, A. A. Balkema, 1995; Tokyo.

Vaid, Y.P. and Thomas, J. [1995], "Liquefaction and post liquefaction behavior of sand," Journal of Geotechnical Engineering, Vol. 121, No. 2, pp. 163-173.

Vinod, J. S. [2006], *"Liquefaction and dynamic properties of granular materials: A DEM approach*", Ph.D. thesis, submitted to Indian Institute of science, Bangalore, India.

Wakabayashi, T. [1957], "Photoelastic method for determination of stress in powdered Mass", *Proceedings of 7th Japan Nat. Congr. Appl. Mech*., pp. 153-158.

Yoshimi, Y; Tokimatsu, K and Hasaka, Y. [1989], Evaluation of liquefaction resistance of clean sands based on high quality undisturbed samples, Soils and Foundations , Vol. 29, No. 1, pp. 93 -104.